Journal of Statistical Physics, Vol. 78, Nos. 3/4, 1995

Patterns of Broken Symmetry in the Impurity-Perturbed Rigid-Disk Crystal

Frank H. Stillinger[1] and Boris D. Lubachevsky[1]

Received May 9, 1994

As a new example of spontaneous pattern formation in many-body systems, we examine the collective means by which a close-packed disk crystal reacts to the presence of a single oversized impurity disk. Computer simulation has been used for this purpose; it creates the jammed impurity-containing packings by a kinetic particle-growth algorithm. Hexagonal primitive cells with periodic boundary conditions were employed, and the "natural" number $3n^2$ of disks (including the impurity) ranged up to 10,800. For impurity diameter 1.2 times that of the other disks, the patterns of observed crystal perturbation displayed several remarkable features. Particle displacements relative to the unperturbed triangular crystal possess local irregularity but long-range coherence. The symmetry of the coherent patterns preserved that of the hexagonal cell for rapid growth, but was lower for slower growth. The final jammed packings contain "rattler" disks of the sort known to appear in random disk packings. Finally, the area increase induced by the presence of a fixed-size impurity appears to grow without bound as the system size (i.e., $3n^2$) itself increases.

KEY WORDS: Pattern selection; symmetry breaking; rigid disks; close packing; crystalline order; point defects; rattlers.

1. INTRODUCTION

It is well known that the densest arrangement of identical rigid disks in the plane is the triangular lattice.[1,2] All disks in this periodic structure are equivalent, and contact six nearest neighbors. An expanded (unjammed) version of this close-packed array appears in the classical rigid-disk system under thermal equilibrium conditions: it is the two-dimensional crystal structure that spontaneously arises when compression of the low-density fluid induces a first-order freezing transition.[3,4] The case of identical rigid

[1] AT & T Bell Laboratories, Murray Hill, New Jersey 07974.

0022-4715/95/0200-1011$07.50/0

spheres in three dimensions may be analogous, but is obscured by the structural multiplicity of regular close-packed arrays[2] and by the absence of a proof that the densest sphere packing is attained in a periodic structure.

This paper examines the geometric disruption of a fully compressed (i.e., jammed) disk crystal produced by an ill-fitting impurity, specifically a single disk somewhat larger than the rest. In view of the simple interlocking of identical disks that is present in their own periodic close-packed array, it is not surprising to find (as we report below) that an impurity can produce very extended patterns of broken symmetry. However, the long-range coherence of the disruption patterns found to coexist with fine-grained local irregularity is a surprising discovery. The strain fields involved in the broken lattice symmetry arise spontaneously as the jammed structures are produced in our calculations, and their long-range coherence features appear to depend on the relative kinetic rate at which the final jammed packing (with embedded impurity) is formed.

It should be emphasized at the outset that our impurity-disrupted crystal configurations arise under *closed* system conditions, that is, fixed numbers of particles as the jammed packing limit is approached. Our procedure thus corresponds roughly to nonequilibrium impurity trapping in real crystalline materials as a result of rapid quenching or compression. An alternate scenario would involve an *open* system with particle exchange to and from a reservoir at controlled chemical potential, and very slow approach to the jamming limit. This latter case would display automatic expulsion to the reservoir of one or more crystal particles from the immediate vicinity of the oversized impurity to accomodate its presence, without producing long-range coherent patterns of disruption.

Examining the influence of an anomalous-size particle in a many-particle system is a well-established strategy in statistical physics. In particular, it is central to the so-called "scaled particle theory" that has been applied both to rigid spheres[5,6] and to rigid disks.[6-8] Furthermore, binary mixtures have been examined both for spheres and for disks, with arbitrary size and concentration ratios, in several publications dealing with various statistical-geometric and condensed-matter phenomena.[9-12] We suspect that the present paper may help to deepen understanding in some of these areas.

Section 2 outlines our computation procedure. Section 3 illustrates its application by considering a small system (27 disks) to establish a few basic concepts. Section 4 presents our major results, involving symmetry-breaking strain patterns in 10,800-disk systems. Section 5 offers some concluding remarks. An appendix is also included to provide an upper-bound estimate of the overall system dilation generated by an oversized impurity.

2. COMPUTATIONAL PROCEDURE

Periodic boundary conditions provide a natural setting for the present study, to eliminate the distracting influence of edge effects. Furthermore, it is desirable to maximize the distance between the perturbing impurity disk in the primary cell and its periodic images in surrounding cells for a given overall system size. This requirement suggests use of a primary cell that has the shape of a regular hexagon, so that it and its periodic images cover the entire plane as a honeycomb structure. When any disk crosses an edge of the primary hexagon into a neighboring image hexagon, a disk image simultaneously enters the primary hexagon across the opposite edge.

With an integer number of particles equal to $3n^2$ $(n = 1, 2, ...)$, it is possible to arrange those particles in the primary hexagon so that their positions and corresponding images form a perfectly periodic infinite triangular array. If all particles were rigid disks with a common diameter a, this is the configuration that permits the largest a value without disk overlap, thus attaining the maximal covering fraction of the plane:

$$\zeta = \pi/(2 \cdot 3^{1/2}) = 0.906899... \tag{2.1}$$

Figure 1 illustrates this standard arrangement for $n = 2$.

As in our earlier studies of random disk packings,[13,14] we generate dynamical trajectories for the disks, accounting for collisions, while all

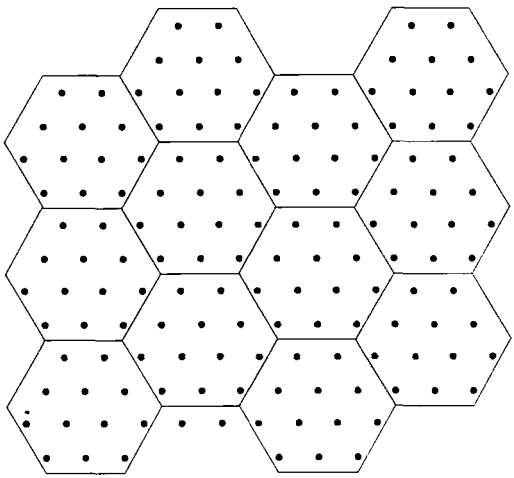

Fig. 1. Honeycomb lattice formed by the regular hexagonal primary cell and its periodic images. Shown as well are positions of 12 particles which, with their periodic replicas, form a triangular array.

disks grow in size at a uniform rate until a jammed (tightly packed) state is achieved. On account of the particle growth, energy is not conserved, but increases with each collision for the system as a whole. In order to assure (at least for large n) that the system dynamical evolution eventually traps the disks in an essentially crystalline (as opposed to amorphous) configuration, the following conditions have always been imposed:

(a) The $3n^2$ disks, including the oversized impurity disk, initially reside on a regular triangular lattice as illustrated in Fig. 1. Because all disks begin the simulation with scaled-down sizes, this configuration involves no overlap.

(b) The impurity disk has been limited in size to no more than $r = 1.4$ times the diameter of the other disks.

(c) The disks are not grown from point particles as in previous studies,[13,14] but start with a substantial fraction of their final diameter. For given size ratio r the initial diameters are chosen so that the oversized impurity very nearly (but not quite) contacts its six neighbors.

Every disk i is initially assigned a velocity with components v_{ix} and v_{iy} uniformly distributed between fixed limits $\pm|v_{\max}|$, so that the mean velocity vanishes and the mean speed is unity. Also, the constant disk-diameter growth rate (scaled proportionately for the impurity) is specified. The ratio of initial diameter growth rate to initial disk translational speed influences the final patterns of crystal disturbance in a substantial way, as will be stressed below.

The mean disk speed and collision rate tend to increase without limit as any given computation proceeds toward jamming.[14] To counteract this phenomenon without significantly influencing the final outcome, disk velocities have been repeatedly scaled downward in the late stages of the computation. Any case is regarded as numerically completed when the covering fraction ζ has stabilized to at least ten significant figures.

3. SMALL-SYSTEM APPLICATIONS

Under the boundary conditions discussed in Section 2, the smallest possible system size ($n = 1$) involves three disks, one of which is larger than the other two. Provided that the diameter ratio r lies in the range

$$1 < r < (2 \cdot 3^{-1/2} - 1)^{-1} = 6.4641... \tag{3.1}$$

this simple periodic system has only a single jammed structure. It is illustrated in Fig. 2. The large "impurity" disk and its images present a

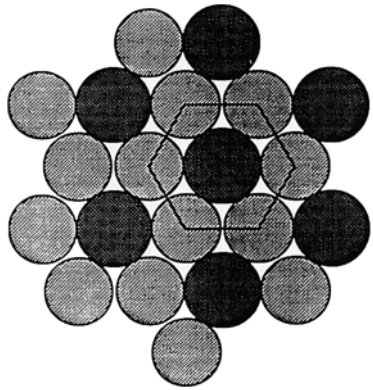

Fig. 2. Unique packing for the periodically replicated three-disk system, provided the size ratio r satisfies Eq. (3.1).

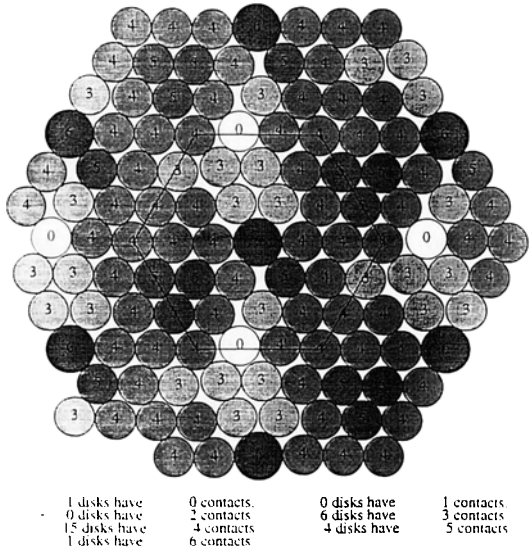

Fig. 3. Twenty-seven disk packing, with central impurity disk 1.2 times the size of the others. Periodic boundary conditions apply across the edges of the hexagonal primitive cell. The number of contacts experienced by particles, defined by Eq. (3.4), is indicated at the center of each disk.

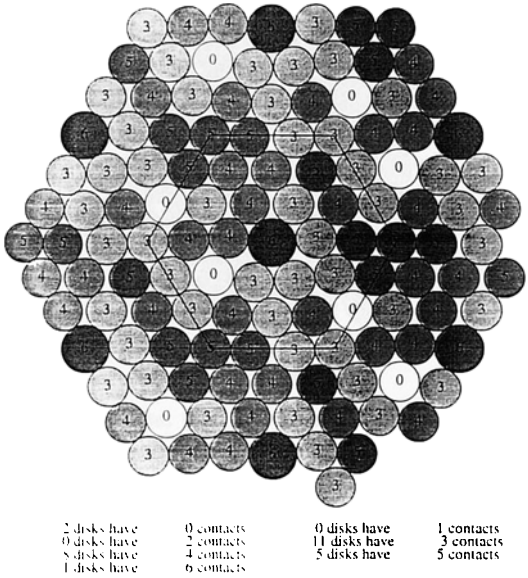

Fig. 4. Alternative disk packing for 27 disks, one of which is an oversized impurity (at center). Conditions are the same as for the packing shown in Fig. 3, except that the initial mean particle speed has been increased by 10^7.

triangular array throughout the plane, while the smaller disks act as "spacers." Each large disk experiences six contacts with smaller disks; smaller disks contact three large disks, but none of their own size. While r remains in the range specified by Eq. (3.1), the covering fraction is

$$\zeta = \frac{2\pi(2+r^2)}{3^{3/2}(1+r)^2} \tag{3.2}$$

Increasing the number of disks in the primary hexagonal cell leads to rather more complicated behavior. For given r, a multiplicity of distinguishable jammed packings appears, the majority of which apparently have symmetry lower than that of Fig. 2. Figures 3 and 4 illustrate this situation for the 27-disk case ($n=3$) and size ratio $r=1.2$, presenting obviously distinct packings. The preparation procedures for these two examples differed only in the initial mean translation speed of the disks compared to their diameter growth rate: 10^{-8} for Fig. 3, 10^{-1} for Fig. 4. The final covered fractions are close, but clearly distinguishable:

$$\begin{aligned} \zeta &= 0.867200086... \quad \text{(Fig. 3)} \\ &= 0.866545725... \quad \text{(Fig. 4)} \end{aligned} \tag{3.3}$$

The disks depicted in Figs. 3 and 4 have been identified by the number of neighbor contacts they experience. Numerically, the contact criterion for any disk pair (i, j) is taken to be

$$[d(i,j) - c(i,j)]/c(i,j) \leqslant 10^{-8} \tag{3.4}$$

where $d(i,j)$ is the distance between the disks (or their images), and $c(i,j)$ is the corresponding collision diameter (which has only two possible values, 1 and 1.1). In both of the cases shown in Fig. 3 and 4 the large impurity disk touches six neighbors; all other disks experience fewer contacts. A necessary criterion for the system to be in a jammed state is that connected pathways consisting of contacting particles must exist across the primary cell between opposite boundaries, and furthermore all particles along the pathways must have three or more contacts. Examination of Figs. 3 and 4 verifies that the disk arrangements shown satisfy this criterion.

It is important to note that both of these 27-disk jammed packings contain "rattlers," i.e., disks with no contacts. In previous studies of the packings of identical disks, rattlers were found to be a characteristic feature of amorphous structures.[13,14] Evidently the forced inclusion of a single oversize impurity disk constitutes a powerful local disruptive influence.

Our survey of the 27-disk system has produced other packings for $r = 1.2$ beyond those illustrated in Fig. 3 and 4. It has also yielded analogous packings for $r = 1.1$ and 1.3. All cases examined exhibited at least one small "rattler" disk.

4. LARGE-SYSTEM APPLICATION

We now pass on to consider a much larger system, containing 10,800 disks ($n = 60$). As before, just one of these will be distinguished by an anomalously large diameter, but its perturbing influence can now spread over a considerably larger area.

One measure of the structural disruption produced by an ill-fitting large disk is the area increase ΔA displayed by the system compared to its unperturbed value ($r = 1$, all disks identical). The appendix derives an upper bound for this quantity; this bound diverges linearly with n for any $r > 1$. For the cases to be examined in this section, involving an impurity with size ratio $r = 1.2$ in the 10,800-particle system, the bound is

$$\Delta A \leqslant 41.002216a^2 \tag{4.1}$$

where as before a is the final nonimpurity disk diameter. This result is based on the outward displacement of triangular disk sectors surrounding the impurity, which maintain their internal contacts. However, the

large-system packings to be discussed actually make much better use of the available space: cooperative disk rearrangements permit substantial reduction in ΔA below the estimate in (4.1).

We now examine the results of four (apparently) representative simulation runs. Their key characteristics are presented in Table I; these include the ratio of disk expansion rate to initial mean speed, and the final ΔA.

Figures 5–8 present representations of the disk displacements occurring for each of the packings, between initial and final configurations. Recall that all disks begin the simulations in a shrunken state, located at the sites of the undistorted triangular lattice. Subsequent disk growth, collisions, and ultimate jamming lead to the final displaced locations. For each of the disks a line segment has been drawn, emanating from the initial position and in the displacement direction, but magnified in length by a factor of ten to facilitate visualization.

The cases illustrated in Figs. 5 and 6 involve disk growth 10^4 times larger than the initial mean particle speed. For those illustrated in Fig. 7 and 8 the corresponding ratio is much smaller, 10^{-3}. In all four cases shown the impurity disk with size ratio 1.2 is located at the center of the primary hexagonal cell.

The large-scale displacement patterns are obviously quite different between the two pairs of cases. The rapid-disk-expansion packings in Fig. 5 and 6 present displacement fields whose coarse-grained description, at least, is sixfold symmetric, radiating outward from the central impurity. Although these first two cases seem visually very similar at the size scale shown, in fact they are geometrically distinct, as the ΔA values listed in Table I verify.

Table I. Characteristic Parameters for Four Simulations, with 10,800 Disks in a Hexagonal Primitive Cell and Periodic Boundary Conditions

Simulation number	1	2	3	4
Figure number	5	6	7	8
Expansion rate/ initial mean speed	10^4	10^4	10^{-3}	10^{-3}
Impurity disk diameter/a	1.2	1.2	1.2	1.2
$\Delta A/a^2$	21.85099	22.09071	20.39012	20.35364
Final pattern type	Six-fold rotation + reflections	Six-fold rotation + reflections	Two reflections	One reflection
Number of rattlers	181	155	65	39

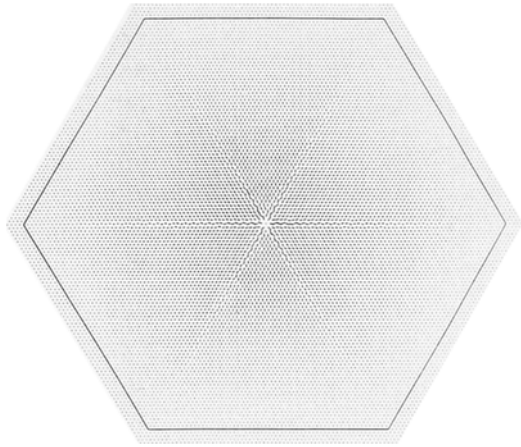

Fig. 5. Displacement pattern for a 10,800-disk packing surrounding an $r = 1.2$ oversized impurity at the center. An expansion factor of ten has been applied to each displacement line to enhance visibility. This is a rapid-disk-growth case (see Table I).

The contrasting slow-disk-expansion conditions employed for Fig. 7 and 8 obviously yield lower coarse-grained symmetry. Figure 7 displays a pair of perpendicular reflection lines passing through the central impurity disk, one passing through opposite vertices of the primitive hexagon, the other bisecting two of its sides. Figure 8 has still lower coarse-grained

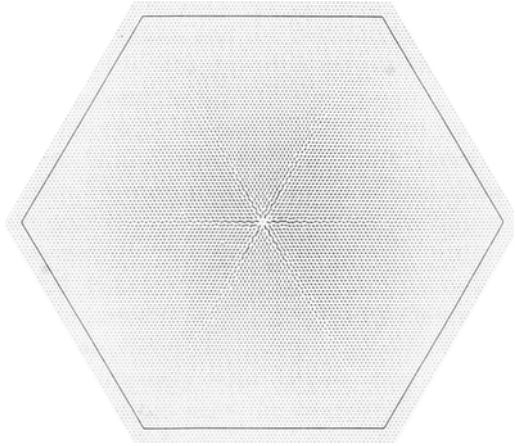

Fig. 6. Displacement pattern for another 10,800-disk packing created under rapid-disk-growth conditions and impurity size ratio $r = 1.2$ (see Table I).

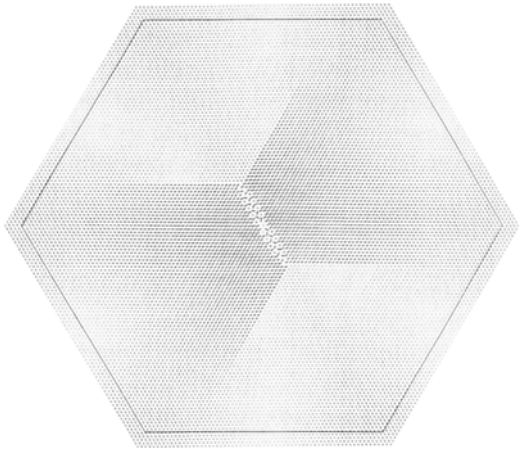

Fig. 7. Displacement pattern for a packing of 10,800 disks created under slow-disk-growth conditions and $r = 1.2$ (see Table I).

symmetry, with only a single side-bisecting reflection line. Once again the packings are distinguishable by their ΔA values listed in Table I.

It seems quite plausible by hindsight that the relative speeds of disk growth rate and of initial translational motion should influence the final packing patterns. If the growth rate is very large as in Fig. 5 and 6, the system becomes jammed before it has a chance to escape the sixfold local

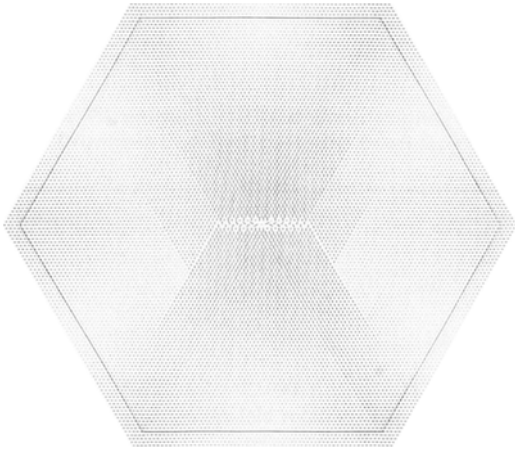

Fig. 8. Displacement pattern for another packing of 10,800 disks with a central $r = 1.2$ impurity, produced with slow-disk-growth conditions.

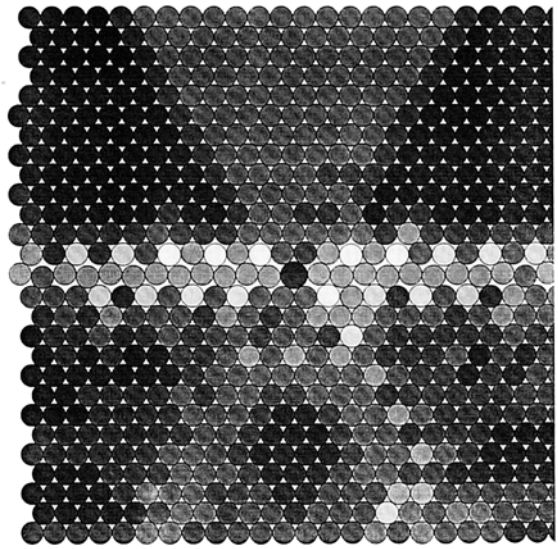

Fig. 9. Arrangement of disks in the central region of the packing depicted in Fig. 8. Particles have been classified by number of contacts according to shading: "rattlers" are white, and increasing darkness indicates more contacts.

symmetry of the initial triangular lattice configuration. But if translational speed dominates disk growth (Figs. 7 and 8), the system has an opportunity to explore available configuration space more fully and to discover geometrically more efficient packings of lower symmetry before jamming sets in. Indeed the ΔA values and the numbers of rattlers listed in Table I are significantly smaller for the slow-disk-expansion conditions than for the rapid-disk-expansion conditions.

Careful examination of the packings produced reveals that patterns of coarse-grained (i.e., large-scale) symmetry have been imposed over fine-grained irregularity. Figure 9 illustrates this feature, showing an expanded view of the disks near the central region of the packing of Fig. 8. Notice in particular the asymmetric distribution of the six rattler particles without contacts (unshaded disks), violating the symmetry of a vertical reflection line. This reflection symmetry is also violated by the small-amplitude zigzag pattern of vertical displacements along the horizontal disk row passing through the central impurity. Our large-system calculations show that rattlers tend to concentrate near the oversize impurity and along grain boundaries.

5. DISCUSSION

The spontaneous appearance of large-scale strain patterns in our impurity-perturbed many-disk system has a wide range of analogs. These include both solid- and liquid- phase phenomena whose late-stage macroscopic patterns can depend sensitively on the initial microscopic state. Specific examples are polycrystalline grain and eutectic patterns produced by melt solidifcation; nonequilibrium fluid phenomena include oscillatory chemical reactions, convective roll patterns, and turbulence.[15] However, none of these share the fundamentally geometric nature of the present case that arises from particle nonoverlap.

The examples we have been able to carry to completion have admittedly been few. For that reason we must be cautious about drawing conclusions. However, the four cases examined with 10,800 disks in Section 4 do suggest that the final large-scale displacement pattern tends to have lower symmetry when initial mean particle speed is large compared to particle growth rate, rather than the reverse. We do not suggest that final symmetry changes discontinuously as this kinetic ratio varies; we presume it is a smooth statistical change, the extreme limits of which are represented by the four cases in Section 4.

We have carried out some limited numerical exploration with disk size ratios differing from 1.2. If the ratio is less than 1.3, the large-scale patterns produced appear to conform to the trend discussed in Section 4. Larger r can lead to coherent but dissymmetric patterns; Fig. 10 supplies an example with $r = 1.4$ and slow disk expansion compared to initial translational speed. Although these computations involving over 10^4 particles are rather demanding, it is desirable to extend the study beyond its present limits.

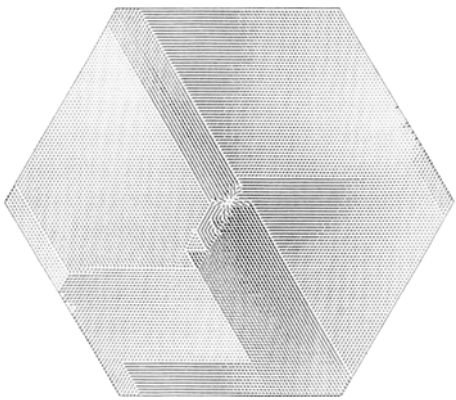

Fig. 10. Displacement pattern for 10,800 disks, with central $r = 1.4$ impurity, and slow-disk expansion.

Such extensions would include nonhexagonal primitive cells; we have carried out preliminary study of 10,864 disks in a square cell, where an oversize impurity also produces coherent large-scale patterns. It would also be illuminating to investigate the three-dimensional case of the close-packed sphere crystal analogously perturbed by an oversize impurity particle.

The ΔA upper bound derived in the appendix, Eq. (A.6), is a linear function of n. While entries in Table I show the disk rearrangement compared to the configuration used to derive this bound reduces ΔA roughly by a factor of 2, it seems hard to escape the conclusion that the least upper bound for disks with $r > 1$ remains a linear function of n. Verification of this assumption and improvement of bound (A.6) remain substantial mathematical challenges, as does the extension to three dimensions.

APPENDIX

When $r = 1$ the "impurity" disk is identical to all others, and the entire collection of $3n^2$ disks can be arranged into a structurally perfect triangular lattice. For simplicity let the common diameter a be unity. The hexagonal cell containing this close-packed arrangement and surrounded by its periodic images will have area

$$A = 3^{3/2}n^2/2 \tag{A.1}$$

If l represents the distance between the center of the primitive hexagon and the midpoint of one of its sides, then regardless of the state of disk packing we always have the relation

$$A = 2 \cdot 3^{1/2}l^2 \tag{A.2}$$

so that in the close-packed state

$$l = 3^{1/2}n/2 \tag{A.3}$$

Now let r increase above 1 while holding the common diameter a of the nonimpurity disks at the previous value 1. The objective is to describe a concerted particle rearrangement that accommodates the impurity growth while avoiding disk overlaps within the primitive hexagon and with image disks. Figure 11 illustrates the scheme to be used. The unit-sized disks are collected into six "tectonic plates" that drift outward from, but maintain contact with, the growing impurity at the center (not shown in Fig. 11 for simplicity). This outward drift requires that the hexagonal primitive cell expand by a corresponding amount. The direction of drift for each of the six plates is perpendicular to a side of the hexagon, and so the

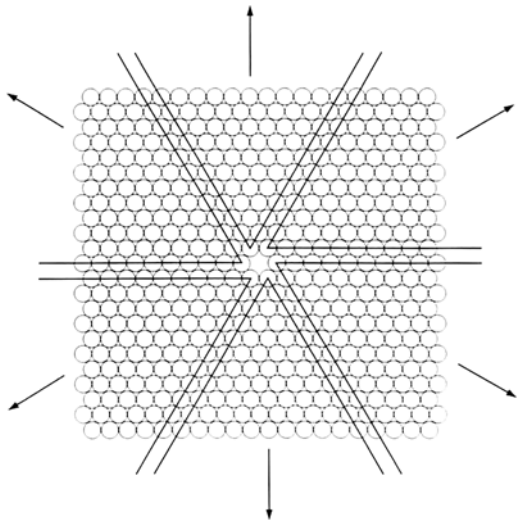

Fig. 11. Tectonic plate motion required to accommodate an expanded impurity disk, not shown, but centered at the vacancy position.

required perfect contact is maintained between disks at the outer edges of those plates and image disks from expanding neighbor hexagonal cells. At the same time, of course, gaps open up between pairs of plates in the primitive hexagon, radiating outward from the central impurity position.

Figure 12 indicates in greater geometric detail how expansion of the central impurity requires outward plate drift, and thus an equal increase in the distance l. One immediately finds that

$$l(r) = 3^{1/2}(n-1)/2 + y(r) \tag{A.4}$$

where $y(r)$ is the unit disk altitude above the impurity center as shown in Fig. 12,

$$y(r) = \tfrac{1}{2}(r^2 + 2r)^{1/2} \tag{A.5}$$

From Eq. (A.2) we can calculate the increase ΔA in system area produced by the impurity:

$$\Delta A = 3^{3/2}\left\{\left[\left(\frac{r^2+2r}{3}\right)^{1/2} - 1\right]n + \frac{1}{2}\left[\left(\frac{r^2+2r}{3}\right)^{1/2} - 1\right]^2\right\} \tag{A.6}$$

This provides an upper bound estimate for ΔA with which the simulation results of the body of the paper can be compared. For general a, expression (A.6) is to be multiplied by a^2.

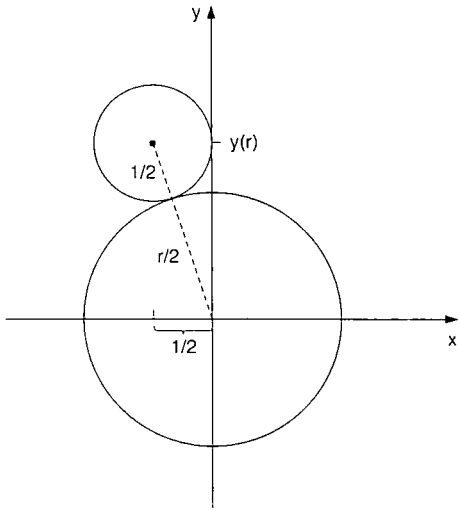

Fig. 12. Geometric constraints determining the magnitude of outward plate motion required by an expanded impurity disk. The y axis is the drift direction for the plate whose inner vertex is the unit disk shown.

A conceivable alternative to the radial plate tectonics just analyzed would be the expulsion of the requisite number of unit-size disks to the outer boundary of the primary cell so as to create a multivacancy large enough to hold the oversize impurity. This alternative would maintain the structural integrity throughout most of the close-packed crystal. But since the expelled disks would have to initiate a new row at the boundary of the primary hexagon, l would have to increase by 1/2. Consequently the corresponding area increase would be

$$\Delta A = 3n + 3^{1/2}/2 \tag{A.7}$$

regardless of how little r might exceed unity. This is a considerably poorer upper bound for our simulation circumstances than is the expression appearing in Eq. (A.6).

REFERENCES

1. C. A. Rogers, *Packing and Covering* (Cambridge University Press, Cambridge, 1964).
2. N. J. A. Sloane, *Sci. Am.* **250**(1):116 (1984).
3. B. J. Alder and T. E. Wainwright, *Phys. Rev.* **127**:359 (1962).
4. J. A. Zollweg and G. V. Chester, *Phys. Rev. B* **46**:11186 (1992).
5. H. Reiss, H. L. Frisch, and J. L. Lebowitz, *J. Chem. Phys.* **31**:369 (1959).

6. H. L. Frisch, *Adv. Chem. Phys.* **6**:229 (1964).
7. E. Helfand, H. L. Frisch, and J. L. Lebowitz, *J. Chem. Phys.* **34**:1037 (1961).
8. M. A. Cotter and F. H. Stillinger, *J. Chem. Phys.* **57**:3356 (1972).
9. L. Fejes Toth, *Regular Figures* (Macmillan, New York, 1964).
10. J. L. Lebowitz and J. S. Rowlinson, *J. Chem. Phys.* **41**:133 (1964).
11. P. W. Leung, C. L. Henley, and G. V. Chester, *Phys. Rev. B* **39**:446 (1989).
12. C. N. Likos and C. L. Henley, *Phil. Mag. B* **68**:85–113 (1993).
13. B. D. Lubachevsky and F. H. Stillinger, *J. Stat. Phys.* **60**:561 (1990).
14. B. D. Lubachevsky, F. H. Stillinger, and E. N. Pinson, *J. Stat. Phys.* **64**:501 (1991).
15. M. C. Cross and P. C. Hohenberg, *Rev. Mod. Phys.* **65**:851 (1993).